Tuning of Sensitivity in Thermochromic Luminescence by Regulating Molecular Rotation Based on Triphenylamine-Substituted *o*-Carboranes

Kenta Nishino, Kazuo Tanaka*, and Yoshiki Chujo

Department of Polymer Chemistry, Graduate School of Engineering, Kyoto University, Katsura, Nishikyo-ku, Kyoto 615-8510, Japan

E-mail: tanaka@poly.synchem.kyoto-u.ac.jp

Abstract

This study demonstrates tuning of sensitivity in thermochromic luminescence from triphenylamine-substituted *o*-carboranes by regulating rotation barriers with the substituent effect. The series of the *o*-carborane dyads with various numbers of methyl substituents were prepared, and their optical properties were compared. Initially, significant dual-emission properties consistent of the locally-excited (LE) state and the induced charge transfer (ICT) state were observed from the solid samples of all dyads. In particular, diverse responses were obtained by cooling from the dyads. The pristine and mono-substituted dyads presented thermally-independent emission during temperature changes, whereas thermochromic luminescence with drastic color change from red to blue was detected originated from alteration of intensity ratios between LE and CT emission bands. From the mechanistic studies including experimental and theoretical investigations, it was clearly shown that the difference in the rotation barrier of the *o*-carborane unit caused by the substituent effect should play a key role in variable sensitivity in luminescent chromic behaviors in temperature change.

Introduction

Development of solid-state emissive organic materials containing boron is a topic with high relevance because of their huge versatility especially on the fabrication of modern optical devices.[1] In particular, by adding stimuli-responsive luminochromic ability, application for wearable and film-type chemical sensors can be expected.[2] To satisfy multiple demands according to the preprogrammed design, luminescence from induced charge transfer (ICT) state is a versatile platform. Because of high sensitivity of the ICT state to environmental factors such as solvent polarity, temperature and viscosity, chemical sensors can be easily constructed.[3] Moreover, the emission bands from locally-excited (LE) and ICT states were occasionally observed from the single materials simultaneously.[4] Based on this dual-emission property, various luminescent colors can be obtained by tuning intensity ratios between these two emission bands.

Conventional organic dyes mostly showed weak emission in the condensed state via aggregation-caused quenching (ACQ) processes, whereas recent reports indicated that modification of aromatics by the *o*-carborane unit is one of effective strategies for avoiding ACQ, followed by observing intense solid-state emission.[5] Therefore, we regard the *o*-carborane unit as the promising solid-state emissive "element-block", which is the minimum functional unit composed of heteroatoms.[6,7] *o*-Carborane is an icosahedral cluster compound composed of 10 boron and 2 carbon atoms linked with three-center-two-electron bonds. Because of electron-deficient nature at the carbons, bright emission from the ICT state can be expressed by the combination with electron-donating units when bonded at the carbon.[8] In particular, it was found from the series of studies with aryl-*o*-carborane dyads that *o*-carborane can work as the efficient solid-state

emissive “element-block”.[9] Even in the solid state, intense ICT emission with almost quantitative emission efficiency was observed.[9] Furthermore, in these dyads, it was shown that rotation at the *o*-carborane unit should be induced in the excited state.[10] As a result, significant emission via twisted intramolecular charge transfer (TICT) was observed in the solid state. According to the computer calculation, it was proposed that mechanical motions at the *o*-carborane unit could be capable in the presence of structural restriction in the condensed state owing to the sphere molecular structure of *o*-carborane.[10] Indeed, under the cooling conditions where intramolecular motions were frozen, rotation was suppressed, resulting in emission only from the locally-excited (LE) state of the aryl moiety. Based on these data, we presumed that luminescent chromic materials can be designed and synthesized by regulating energy barriers in the rotation of the *o*-carborane unit. Especially, by modulating emission intensity ratios between LE and TICT states, drastic color changes were expected. To prove validity of this idea, we designed electron-donor-modified *o*-carborane dyads consisting of triphenylamine because of significant luminescent properties in solid.[11]

Herein, controls of stimuli-responsive luminescent chromic behaviors in the solid state are described with the triphenylamine-substituted *o*-carborane dyads. Based on the idea for obtaining dual-emission property by modulating rotation barriers at the *o*-carborane unit, the substituent effect was employed. From the optical measurements, it was clearly shown that thermochromic luminescence was accomplished with the solid sample of the synthesized dyads. Furthermore, it was shown that sensitivity in luminescent thermochromic behaviors was varied. From the mechanistic studies, it was suggested that the degree of rotation during the TICT process should be altered by the substituent effect.

Finally, both thermally-resistant emission and drastic color change between blue and red can be obtained from the single dyad system.

Results and Discussion

Three types of the triphenylamine-substituted *o*-carborane dyads were designed (Scheme 1). The dyad **3a** is a basic structure. Because of less steric hindrance around the *o*-carborane unit, it was presumed that free rotation frequently occurred both in the ground and excited states. As a result, dual emission properties were expected. **3b** and **3c** were supposed to mainly form the twisted and planar conformations between the C−C bond in the *o*-carborane unit and the molecular plane of the triphenylamine moiety because of structural restriction caused by steric hindrances of the methyl substituents, respectively. It was assumed that degree of rotation could be suppressed by the substituent effects, and different optical properties and responsivity toward heating were proposed. Synthetic routes are shown in Scheme 2. Initially, *p*-bromo-*o*-carboranylbenzene derivatives **2a–c** were obtained via the alkyne insertion reaction with decaborane.[12] Then, triphenylamine-*o*-carborane dyads **3a-c** were synthesized via the Buchwald–Hartwig cross coupling reaction.[13] All compounds were characterized by the ^{1}H, ^{11}B and ^{13}C NMR spectra and HRMS measurements. The products showed good stability and solubility in common organic solvents such as $CHCl_3$, CH_2Cl_2, tetrahydrofuran (THF) and benzene. Thus, we concluded that the products should have the designed structures and enough stability for performing the series of measurements.

Schemes 1 and 2

UV–vis absorption spectra of **3a**−**c** in the octane solution at 298 K are shown in Figure 1a. The optical properties are listed in Table 1. All samples showed the broad absorption bands with the peaks around 300 nm attributable π−π* transition at the triphenylamine

moiety.[11,14] The peak shifts were induced by connecting with *o*-carborane although the width of the shifts were small. It is likely that extension of π-conjugation should occur through σ*−π* interaction on the C−C bond in *o*-carborane. Next, photoluminescence (PL) spectra of the compounds were measured in the solution state (Figures 1b). In octane, **3a** showed the emission bands around 370 and 560 nm. The emission band around 370 nm was identical to that of triphenylamine.[11,14] Moreover, by increasing solvent polarity, the emission band around 370 nm was hardly shifted, and only the emission band around 560 nm was red-shifted (Figure S1). These facts indicate that the emission bands around 370 and 560 nm are assigned as the LE and ICT emission, respectively.[15] The dual-emission property was also observed from **3b** and **3c** although intensity at the LE emission was extremely low. In the presence of the substituents, free rotation could be disturbed. Reverse transition from the ICT state to the LE state should be suppressed, followed by large emission bands with the ICT character.

To investigate dual emission properties in detail, temperature dependency was investigated on optical properties (Figures S2 and S3). Absorption bands were slightly influenced by temperature changes, while the relative intensities of the ICT emission compared to the LE emission of **3a** and **3b** decreased by heating from 293 K to 353 K and by cooling from 283 K to 253 K, respectively. In contrast, the relative intensity of the ICT emission of **3c** increased by heating to 353 K. Based on these data, the Stevens–Ban plots were prepared (Figure S4).[16] From the fitting lines, rotation energies (E_a) and energy gaps between LE and ICT states (ΔH) can be estimated according to the literature.[16] The E_a values of **3a**, **3b** and **3c** were 3.4 kJ/mol, 9.1 kJ/mol and 10.1 kJ/mol, respectively. In addition, ΔH values of **3a** and **3b** were estimated as 4.4 kJ/mol and 5.4

kJ/mol, respectively. These data mean that the rotation barrier in the excited state of **3c** is the largest in three carboranes. It is likely that the largest steric hindrances from dual methyl substituents in **3c** should contribute to increasing rotation energy (Figure S5). In addition, small values of ΔH were obtained from the plots. This means that in the excited state, rotation should be capable.

It is known that the planar and twist conformations are favorable for exhibiting LE and ICT or TICT emission, respectively.[10] Furthermore, molecular conformation can be evaluated from the emission property. Next, luminescent spectra in 2-methylTHF solutions at 77 K were measured (Figure S6). Three emission bands with the peaks at 360, 450 and 640 nm were observed from **3a**. Emission peaks around 360 and 640 nm were assigned to the transitions from the LE and ICT states, respectively. The emission band around 450 nm showed long decay time (4.2 ms) and corresponded to phosphorescence of triphenylamine (Figure S7).[11] **3b** showed the large ICT emission band around 600 nm, meanwhile **3c** presented the LE emission around 370 nm. These results suggest that the most stable molecular structure of **3b** and **3c** should be the twisted and planar conformations in the ground state, respectively.[10]

Solid-state emission properties were measured with the dyads (Figure 2). **3a** and **3c** demonstrated the dual-emission behaviors at room temperature similarly to those in the solution state, while **3b** showed a large emission band around 590 nm attributable to the ICT emission. Moreover, absolute photoluminescence quantum yields (Φ_{PL}) of **3a, 3b** and **3c** of the ICT emission were 0.035, 0.648 and 0.060, respectively (Table 1). According to the literature, these strong emission bands from the ICT state and high quantum yields

were induced by preventing the rotation at the *o*-carborane unit by the methyl group at the carbon atom in *o*-carborane.[9] The quantum yield of **3b** was significantly higher than those of others. This fact was caused by the structural immobilization at the twisted conformation in which the ICT transition is favorable. To check validity of this speculation, the PL spectra with solid samples were carried out at 77 K.[17]

At 77 K, solid sample of **3b** showed only the large emission band with the peak at 600 nm attributable to the ICT emission. Although the emission bands around 600 nm were also observed in **3a** and **3c**, the emission bands attributable to the LE emission were obtained. The solid sample of **3b** was stable at the twisted conformation, and the ICT emission was obtained. In the solid sample of **3a** and **3c**, both conformations could exist, and subsequently emission bands from both states should be simultaneously observed. At 77 K, **3c** showed the large emission band with the peak at 390 nm attributable to the LE emission. Rotation of the *o*-carborane unit was efficiently restricted by the substituent effect, and the existing ratio of the planar conformation could increase. Thereby, the clear dual emissive property should appear at 77 K. Finally, emission color was dramatically changed from red to blue by cooling.

To support their optical properties, theoretical evaluation was performed. Initially, their optimized conformations were estimated, and molecular orbitals were calculated by using density functional theory (DFT) and time-dependent DFT (TD-DFT) at the CAM-B3LYP/6-31+G(d,p)//B3LYP/6-31G(d) level by using Gaussian09 program in the ground and excited states, respectively.[18] The length of the C−C bond in *o*-carborane and the dihedral angle between the C−C bonds in *o*-carborane and triphenylamine were denoted

as *l* and *φ*, respectively. It was proposed that two conformations with similar total energy levels should exist in the ground state of the dyads (Figures S8 and S9). Representatively in **3a** and **3c**, the planar and twisted conformations were obtained from structural optimization. The results from TD-DFT calculation showed good agreement with the absorption spectra (Table S1). Moreover, from evaluation of electronic structures, the corresponding results were obtained with the previous reports on the *o*-carborane dyads.[10] In summary, HOMOs were located at the triphenylamine moiety, and LUMOs were delocalized through whole molecules. Similar orbital shapes of HOMOs and LUMOs were obtained in the planar and twisted conformations. It was confirmed that twisted conformations showed the σ*−π* conjugation involving the phenyl ring and the C−C bond in *o*-carborane. Planar conformations showed the σ*−π* conjugation involving the phenyl ring and the C−B bond in *o*-carborane. The LUMO energy level of **3a** was more stable than that of triphenylamine because of extension of conjugated system. This result strongly supports the above speculation on the red-shifted absorption band of **3a** toward triphenylamine. **3b** and **3c** showed similar electronic orbitals. Therefore, similar absorption bands were also observed.

Next, to gather information on emission properties, the quantum calculation was carried out with the excited molecules. Molecular orbitals and energy levels in each conformation were calculated by using a TD-DFT method (Figure 3). From the peak positions in the PL spectra, the $S_1'-S_0'$ transition was assigned to the transition between HOMO and LUMO. According to the localization of molecular orbitals on the dyads, it was proposed that transitions in the twisted conformation had the ICT character, meaning that the red emission should be obtained from the HOMO−LUMO transition in the

twisted conformation. Molecular orbitals were mainly localized at the *o*-carborane units in LUMOs in the twisted conformation, meanwhile molecular orbitals were largely found at the triphenylamine moieties in HOMOs. In the planar conformation, molecular orbitals constantly existed at the triphenylamine moieties in LUMOs although localization patterns in the whole molecules were varied. These tendencies were often observed from the luminescent molecules with the ICT character. Furthermore, in the planar conformation, the C−C bond length in *o*-carborane was 1.64 Å, while the C−C bond length was elongated to 2.38 Å in the twisted conformation. This bond elongation was also suggested in the previous report on the *o*-carborane derivatives having the emission property with the ICT character.[19]

Finally, to explain sensitivity differences in thermochromic luminescence, further calculations were performed. The energy diagrams of **3a−c** with different dihedral angles (φ) in the absorption S_0–S_1 and emission S_1'–S_0' transitions were estimated (Figure S10). Schematic illustrations are presented in Figure 4. In the S_0 (black dots) and S_1' (gray dots) states, energies of **3a** were almost constant regardless of dihedral angles. This result suggests that the rotation barrier should be very small, and both planar and twisted conformations can be formed in the ground and excited states. Indeed, in the solid state, the dual emission behavior was observed (Figure 4a). In contrast, the energy diagrams of **3b** and **3c** were influenced by the dihedral angle. The energy of **3b** in S_0 and S_1' states became lower by increasing the dihedral angle. Since steric hindrance of the methyl group should be minimized, the twisted conformation has the lower energy compared to the planar one. In Figure 4b, the ICT emission bands derived from the twisted state were detected. The energy level of **3c** around 0° was more stable than that around 90° at the S_0

state with the rotation barrier around 30–80°, whereas the twisted conformation was the most stable at the S1' state. These results suggest that **3c** prefers to form the planar conformation in the ground state, meanwhile the twisted conformation is favorable in the excited state. These showed good agreement with the data in Figure 4c. At room temperature, conformational change from planar to twisted conformation proceeded in the excited state, resulting in intense red emission from the ICT state. On the other hand, the LE emission in the blue region originated from the planar conformation was enhanced in the solid state at 77 K. Therefore, clear thermochromic luminescence from red to blue by cooling was accomplished. From these data, it was suggested that sensitivity in thermochromic luminescence can be tuned by introducing the substituents via regulation of degree of molecular rotation at the *o*-carborane unit.

Conclusion

By introducing the substituents around the *o*-carborane unit in the triphenylamine-modified dyads, the height of rotation barriers was altered. As a consequence, dual-emissive properties were obtained from the solid samples of the dyads. Especially, not only intensity ratios between the LE and ICT emission bands in dual emission behaviors but also temperature dependency of luminescent chromism can be tuned. Finally, both solid-state thermochromic luminescence and thermally-resistant emission properties were realized with the same molecular skeleton. Our concept could be valid for developing advance luminescent chromic materials according to preprogrammed molecular design.

ACKNOWLEDGMENT

This work was partially supported by the Asahi Glass Foundation (for K.T.) and a Grant-in-Aid for Scientific Research (B) (JP17H03067) and (A) (JP17H01220), for Scientific Research on Innovative Areas “New Polymeric Materials Based on Element-Blocks (No.2401)” (JP24102013) and for Challenging Research (Pioneering) (JP18H05356).

References

1. K. Tanaka, Y. Chujo, *Macromol. Rapid Commun*. **2012**, **33**, 1235–1255.
2. a) K. Tanaka, Y. Chujo, *NPG Asia Mater*. **2015**, *7*, e223; b) M. Gon, K. Tanaka, Y. Chujo, *Bull. Chem. Soc. Jpn*. **2019**, *92*, 7−18.
3. A. Ito, R. Kurata, K. Tanaka, M. Gon, Y. Chujo, *J. Org. Chem*. **2017**, *82*, 5111−5121.
4. a) T. Matsumoto, H. Takamine, K. Tanaka, Y. Chujo, *Mater. Chem. Front*. **2017**, *1*, 2368−2375; b) M. Gon, K. Kato, K. Tanaka, Y. Chujo, *Mater. Chem. Front*. **2019**, *3*, 1174−1180.
5. a) R. Furue, T. Nishimoto, I. S. Park, J. Lee, T. Yasuda, *Angew. Chem. Int. Ed*. **2016**, *55*, 7171−7175; b) S. X. Wu, J. Guo, Y. Cao, J. Zhao, W. Jia, Y. Chen, D. Jia, *Chem. Sci*. **2018**, *9*, 5270−5277; c) M. R. Son, Y.-J. Cho, S.-Y. Kim, H.-J. Son, D. W. Cho, S. O. Kang, *Phys. Chem. Chem. Phys*. **2017**, *19*, 24485−24492; d) D. Tu, P. Leong, S. Guo, H. Yan, C. Lu, Q. Zhao, *Angew. Chem. Int. Ed*. **2017**, *56*, 11370–11374; e) Y. Chen, J. Guo, X. Wu, D. Jia, F. Tong, *Dyes Pigments* **2018**, *148*, 180−188; f) A. Ferrer-Ugalde, J. Cabrera-González, E. J. Juárez-Pérez, F. Teixidor, E. Pérez-Inestrosa, J. M. Montenegro, R. Sillanpää, M. Haukka, R. Núñez, *Dalton Trans*. **2017**, *46*, 2091−2104; g) Z. Wang, T. Wang, C. Zhang, M. G. Humphrey, *Phys. Chem. Chem. Phys*. **2017**, *19*, 12928−12935; h) X. Li, Y. Yin, H. Yan, C. Lu, *Chem. Asian J*. **2017**, *12*, 2207–2210; i) X. Li, H. Yan, Q. Zhao, *Chem. –Eur. J*. **2016**, *22*, 1888−1898; j) S. Mukherjee, P. Thilagar, *Chem. Commun*. **2016**, *52*, 1070−1093; k) L. Böhling, A. Brockhinke, J. Kahlert, L. Weber, R. A. Harder, D. S. Yufit, J. A. K. Howard, J. A. H. MacBride, M. A. Fox, *Eur. J. Inorg. Chem*. **2016**, 403−412; l) L. Weber, J. Kahlert, R. Brockhinke, L.

Böhling, J. Halama, A. Brockhinke, H.-G. Stammler, B. Neumann, C. Nervi, R. A. Harder, M. A. Fox, *Dalton Trans*. **2013**, *42*, 10982−10996; m) J. Kahlert, L. Böhling, A. Brockhinke, H.-G. Stammler, B. Neumann, L. M. Rendina, P. J. Low, L. Weber, M. A. Fox, *Dalton Trans*. **2015**, *44*, 9766−9781; n) B. H. Choi, J. H. Lee, H. Hwang, K. M. Lee, M. H. Park, *Organometallics* **2016**, *35*, 1771−1777; o) M. Eo, M. H. Park, T. Kim, Y. Do, M. H. Lee, *Polymer* **2013**, *54*, 6321−6328; p) T. Kim, H. Kim, K. M. Lee, Y. S. Lee, M. H. Lee, *Inorg. Chem*. **2013**, *52*, 160−168; q) J. J. Peterson, A. R. Davis, M. Were, E. B. Coughlin, K. R. Carter, *ACS Appl. Mater. Interfaces* **2011**, *3*, 1796−1799; r) D. Tu, P. Leong, Z. Li, R. Hu, C. Shi, K. Y. Zhang, H. Yan, Q. Zhao, *Chem. Commun*. **2016**, *52*, 12494−12497; s) W. Zhang, Y. Luo, Y. Xu, L. Tian, M. Li, R. He, W. Shen, *Dalton Trans*. **2015**, *44*, 18130−18137; t) L. Zhu, X. Tang, Q. Yu, W. Lv, H. Yan, Q. Zhao, W. Huang, *Chem. Eur. J*. **2015**, *21*, 4721−4730; u) K.-R. Wee, Y.-J. Cho, S. Jeong, S. Kwon, J.-D. Lee, I.-H. Suh, S. O. Kang, *J. Am. Chem. Soc*. **2012**, *134*, 17982−17990; v) A. V. Marsh, N. J. Cheetham, M. Little, M. Dyson, A. J. P. White, P. Beavis, C. N. Warriner, A. C. Swain, P. N. Stavrinou, M. Heeney, *Angew. Chem. Int. Ed*. **2018**, *57*, 10640−10645; w) R. Núñez, M. Tarrés, A. Ferrer-Ugalde, F. F. de Biani, F. Teixidor, *Chem. Rev*. **2016**, *116*, 14307−14378; x) R. Núñez, I. Romero, F. Teixidora, C. Viñas, *Chem. Soc. Rev*. **2016**, *45*, 5147−5173.

6. a) Y. Chujo, K. Tanaka, *Bull. Chem. Soc. Jpn.* **2015**, *88*, 633−643; b) M. Gon, K. Tanaka, Y. Chujo, *Polym. J*. **2018**, *50*, 109−126.

7. a) K. Nishino, K. Hashimoto, K. Tanaka, Y. Morisaki, Y. Chujo, *Tetrahedron Lett*. **2016**, *57*, 2025−2028; b) K. Nishino, K. Uemura, K. Tanaka, Y. Chujo, *New J. Chem*. **2018**, *16*, 4210−4214; c) K. Nishino, Y. Morisaki, K. Tanaka, Y. Chujo,

New J. Chem. **2017**, *15*, 10550−10554; d) H. Naito, K. Uemura, Y. Morisaki, K. Tanaka, Y. Chujo, *Eur. J. Org. Chem*. **2018**, 1885−1890; e) K. Nishino, K. Uemura, K. Tanaka, Y. Morisaki, Y. Chujo, *Eur. J. Org. Chem*. **2018**, 1507−1512; f) K. Nishino, K. Hashimoto, K. Tanaka, Y. Morisaki, Y. Chujo, *Sci. China Chem*. **2018**, *61*, 940−946; g) K. Nishino, H. Yamamoto, K. Tanaka, Y. Chujo, *Asian J. Org. Chem*. **2017**, *6*, 1818−1822; h) J. Ochi, K. Tanaka, Y. Chujo, *Eur. J. Org. Chem*. **2019**, 2984−2988; i) K. Nishino, K. Tanaka, Y. Morisaki, Y. Chujo, *Chem. Asian J*. **2019**, *14*, 789−795.

8. a) Y.-J. Cho, S.-Y. Kim, M. Cho, W.-S. Han, H.-J. Son, D. W. Cho, S. O. Kang, *Phys. Chem. Chem. Phys*. **2016**, *19*, 9702−9708; b) S.-Y. Kim, Y.-J. Cho, G. F. Jin, W.-S. Han, H.-J. Son, D. W. Cho, S. O. Kang, *Phys. Chem. Chem. Phys*. **2015**, *17*, 15679−15682; c) Z. Wang, P. Jiang, T. Wang, G. J. Moxey, M. P. Cifuentes, C. Zhang, M. G. Humphrey, *Phys. Chem. Chem. Phys*. **2016**, *18*, 15719−15726; d) S. Kwon, K.-R. Wee, Y.-J. Cho, S. O. Kang, *Chem. Eur. J*. **2014**, *20*, 5953−5960.

9. a) H. Naito, K. Nishino, Y. Morisaki, K. Tanaka, Y. Chujo, *J. Mater. Chem. C* **2017**, *4*, 10047−10054; b) K. Nishino, H. Yamamoto, K. Tanaka, Y. Chujo, *Org. Lett*. **2016**, *18*, 4064−4067; c) H. Naito, K. Nishino, Y. Morisaki, K. Tanaka, Y. Chujo, *Chem. Asian J*. **2017**, *12*, 2134−2138.

10. H. Naito, K. Nishino, Y. Morisaki, K. Tanaka, Y. Chujo, *Angew. Chem. Int. Ed.* **2017**, *56*, 254–259.

11. K. Nishino, K. Uemura, K. Tanaka, Y. Chujo, *Molecules* **2017**, *22*, 2009−2018.

12. K. Kokado, A. Nagai, Y. Chujo, *Macromolecules* **2010**, *43*, 6463−6468.

13. F. Paul, J. Patt, J. F. Hartwig, *J. Am. Chem. Soc.* **1994**, *116*, 5969−5970.

14. a) M. Uebe, A. Ito, Y. Kameoka, T. Sato, K. Tanaka, *Chem. Phys. Lett*. **2015**, *633*, 190−194; b) Y. Kameoka, M. Uebe, A. Ito, T. Sato, K. Tanaka, *Chem. Phys. Lett*. **2014**, *615*, 44−49.

15. a) H. Mori, K. Nishino, K. Wada, Y. Morisaki, K. Tanaka, Y. Chujo, *Mater. Chem. Front*. **2018**, *2*, 573–579; b) K. Nishino, H. Yamamoto, K. Tanaka, Y. Chujo, *Chem. Asian J*. **2019**, *14*, 1577−1581.

16. B. Stevens, M. I. Ban, *Trans. Faraday Soc.* **1964**, *60*, 1515−1523.

17. G. U. Bublitz, S. G. Boxer, *J. Am. Chem. Soc.* **1998**, *120*, 3988–3992.

18. Gaussian 09, Revision **D.01**, M. J. Frisch *et al.* Gaussian, Inc., Wallingford CT, 2009.

19. a) I. V. Glukhov, M. Y. Antipin, K. A. Lyssenko, *Eur. J. Inorg. Chem*. **2004**, *7*, 1379−1384; b) K. Tanaka, K. Nishino, S. Ito, H. Yamane, K. Suenaga, K. Hashimoto, Y. Chujo, *Faraday Discuss.* **2017**, *196*, 31−42.

Figures and Tables

Scheme 1. Molecular structures of *o*-carborane and triphenylamine-*o*-carborane dyads **3a–3c**

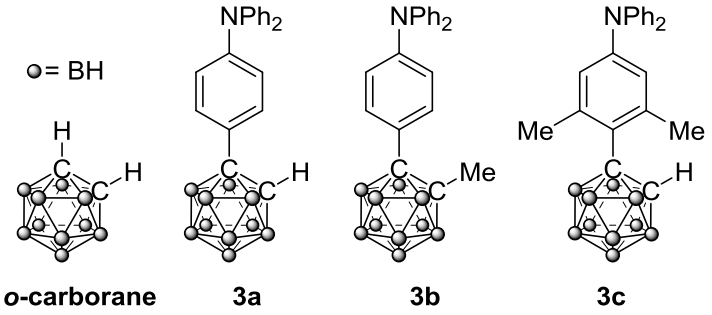

Scheme 2. Synthesis of triphenylamine–*o*-carborane dyads

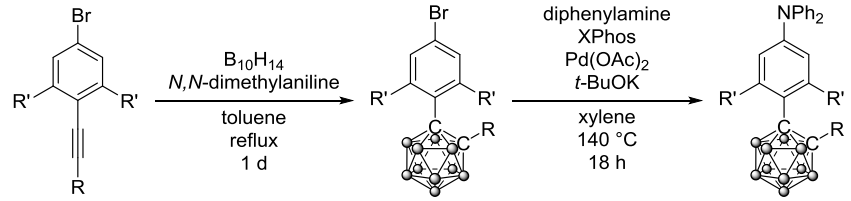

1a-c **2a-c** **3a-c**

1a: R = H, R' = H — **2a**: 70% — **3a**: 9%
1b: R = Me, R' = H — **2b**: 51% — **3b**: 43%
1c: R = H, R' = Me — **2c**: 5% — **3c**: 4%

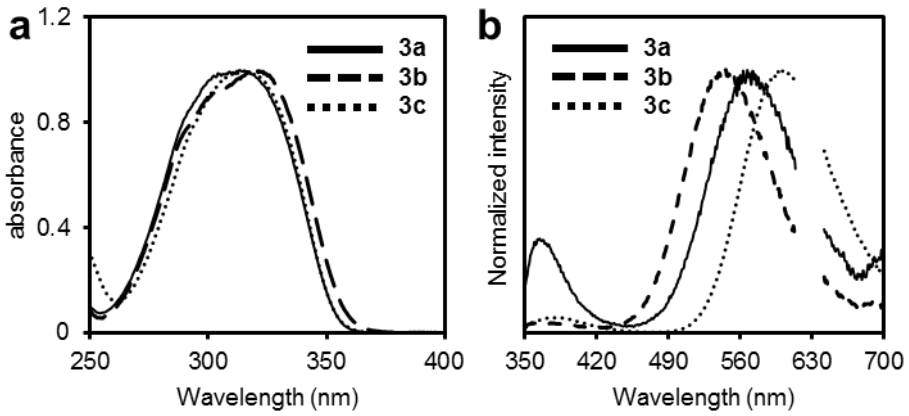

Fig. 1 (a) UV–vis absorption and (b) normalized PL spectra of **3a**–**c** in the octane solutions with the concentration at 1.0×10^{-5} M.

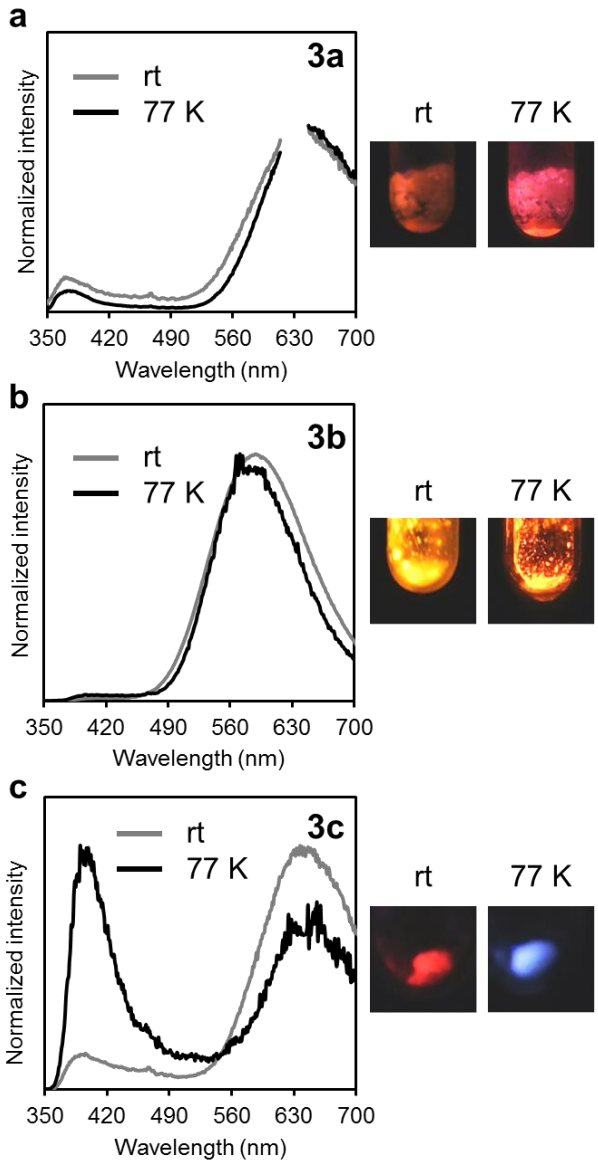

Fig. 2 PL spectra of the solid samples at room temperature and 77 K and pictures under UV irradiation (365 nm).

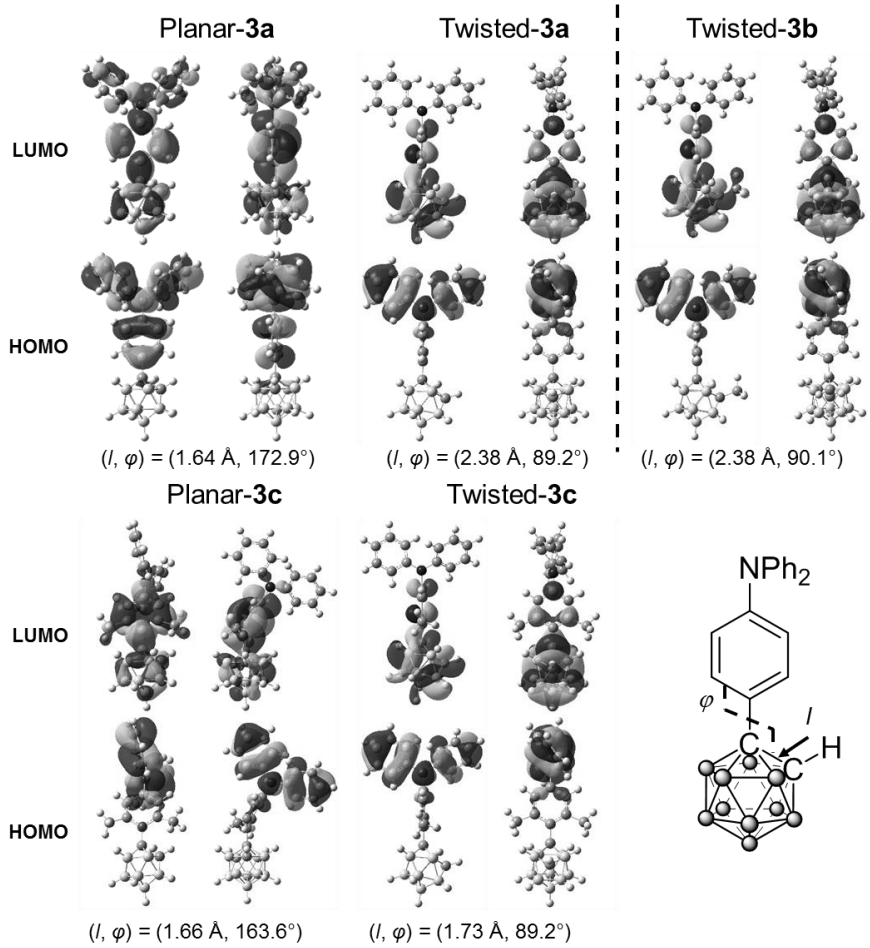

Fig. 3 Calculated molecular orbitals in the transitions of **3a**–**c** in the excited state.

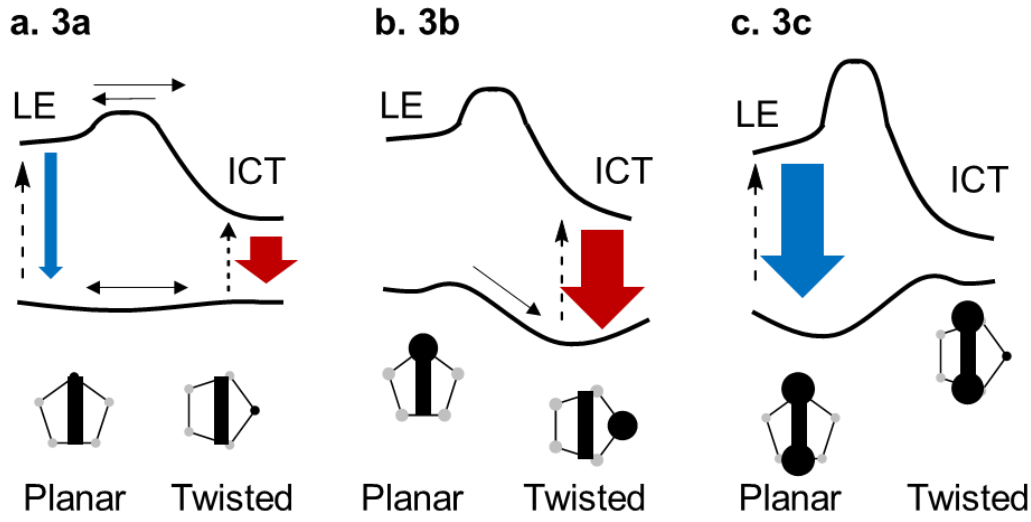

Fig. 4 Proposed emission mechanisms of **3a**–**c** in solid. Black bar means the benzene ring. Small black and grey ball means the C-H and B-H, respectively. Large black ball means the methyl group.

Table 1. Optical properties of **3a**–**c**

compound	λ_{abs} (nm)[a]	$\lambda_{em,rt}$ (nm)[b]	$\lambda_{em,rt}$ (nm)[c]	Φ_{PL}[d]	$\lambda_{em,77K}$ (nm)[e]	$\lambda_{em,rt}$ (nm)[f]	Φ_{PL}[d]	$\lambda_{em,77K}$ (nm)[f]	E_a (kJ/mol)	ΔH (kJ/mol)	$E_a+\Delta H$ (kJ/mol)
3a	314	374, 557	364, 567	<0.01	361, 424, 662	372, 635	0.04	372, 649	3.4	4.4	7.8
3b	319	548	608	<0.01	365, 687	589	0.65	591	9.1	5.4	14.5
3c	323	389, 609	372	<0.01	386	382, 637	0.60	400, 648	10.1	–	–

[a]1.0×10^{-5} M in octane at room temperature. [b]1.0×10^{-5} M in octane at room temperature with the excitation light at λ_{abs}. [c]1.0×10^{-5} M in 2-methylTHF at room temperature with the excitation light at λ_{abs}. [d]Determined as an absolute value with the integration sphere method. [e]1.0×10^{-5} M in 2-methylTHF at 77 K with the excitation light at λ_{abs}. [f]Measured in the solid state with the excitation light at λ_{abs}.

Graphical Abstract

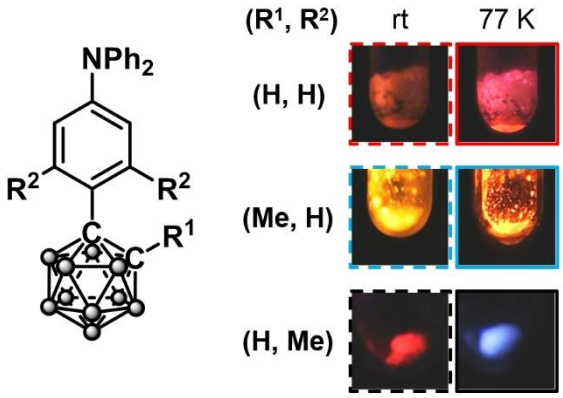

Supporting Information

Tuning of Sensitivity in Thermochromic Luminescence by Regulating Molecular Rotation Based on Triphenylamine-Substituted *o*-Carboranes

Kenta Nishino, Kazuo Tanaka*, and Yoshiki Chujo

Department of Polymer Chemistry, Graduate School of Engineering, Kyoto University, Katsura, Nishikyo-ku, Kyoto 615-8510, Japan

E-mail: tanaka@poly.synchem.kyoto-u.ac.jp

Experimental section

General

^{1}H, ^{13}C, and ^{11}B NMR spectra were recorded on a JEOL JNM-EX400 instrument at 400, 100, and 128 MHz, respectively. The ^{1}H and ^{13}C chemical shift values were expressed relative to Me_4Si as an internal standard. The ^{11}B chemical shift values were expressed relative to $BF_3 \cdot Et_2O$ as an external standard. High-resolution mass spectra (HRMS) were obtained on a Thermo Fisher Scientific EXACTIVE spectrometer for atmospheric pressure chemical ionization (APCI). Analytical thin-layer chromatography (TLC) was performed with silica gel 60 Merck F254 plates. Column chromatography was performed with Wakogel C-300 silica gel. UV–vis absorption spectra were obtained on a SHIMADZU UV3600 spectrophotometer. Photoluminescence (PL) spectra were obtained on a Horiba FluoroMax-4 luminescence spectrometer. Absolute PL quantum efficiencies (Φ_{PL}) were determined using a Horiba FL-3018 Integrating Sphere.

Materials

All synthetic procedures were performed under Ar atmosphere. Decaborane ($B_{10}H_{14}$), *N*,*N*-dimethylaniline, XPhos, *p*-bromoethynylbenzene, toluene, diphenylamine, $Pd(OAc)_2$, *t*-BuOK and xylene were purchased and used without other purification. *p*-Bromomethylethynylbenzene[1] and *p*-bromo-*m*,*m*-dimethylethynylbenzene[2] were synthesized according to the literature.

Synthetic procedures

General synthesis of *p*-bromo-(*o*-carborane-1-yl)benzene, 2a–c

Decaborane (1.15 eq.) was dissolved in toluene (10 mL for 1.0 mmol of ethynyl derivative) containing *N*,*N*-dimethylaniline (1.8 eq.) under Ar atmosphere. The mixture was stirred at room temperature for 1 h, and then *p*-bromoethynylbenzene derivative (**1a**−**c**) (1.0 eq.) was added.

Subsequently, the mixture was refluxed for 1 d. After cooling to room temperature, insoluble products were removed by filtration, and the solvent was evaporated. The residue was purified by column chromatography on a silica gel (hexane/$CHCl_3$ v/v = 9:1). After evaporation of solvents, the desired product was isolated with recrystallization from $CHCl_3$/MeOH.

2a.

White crystal (70%). ^{1}H NMR (400 MHz, $CDCl_3$): δ (ppm) 7.47 (dt, 1H, *J* = 8.8, 2.2 Hz, Ar–*H*), 7.35 (dt, 1H, *J* = 8.8, 2.3 Hz, Ar–*H*), 3.90 (s, 1H, carborane_C–*H*), 3.49–1.52 (br, 13H, B–*H*). ^{13}C NMR (100 MHz, $CDCl_3$): δ (ppm) 132.6, 132.0, 129.2, 124.6, 75.5, 60.2. ^{11}B NMR (128 MHz, $CDCl_3$): δ (ppm) –1.3, –2.4, –3.6, –4.8, –8.2, –9.5, –10.2, –10.8, –11.4, –12.0, –13.3. HRMS (APCI$^-$): Calcd. for $C_8H_{15}B_{10}Br$ $(M+Cl)^-$ m/z 335.1034, found m/z 335.1024.

2b.

White crystal (51%).^{1}H NMR (400 MHz, $CDCl_3$): δ (ppm) 7.52 (d, 4H, *J* = 2.2 Hz, Ar–*H*), 3.50–1.57 (br, 13H, B–*H*, CH_3). ^{13}C NMR (100 MHz, $CDCl_3$): δ (ppm) 132.6, 132.1, 130.1, 125.5, 81.1, 77.2, 23.2. ^{11}B NMR (128 MHz, $CDCl_3$): δ (ppm) –2.3, –3.8, –5.1, –8.7, –9.6, –10.8. HRMS (APCI$^-$): Calcd. for $C_9H_{17}B_{10}Br$ $(M)^-$ m/z 314.1502, found m/z 314.1506.

2c.

White crystal (5%).^{1}H NMR (400 MHz, $CDCl_3$): δ (ppm) 7.22 (2H, s, Ar–*H*), 5.06 (s, 1H, carborane_C–*H*) 2.52–1.56 (br, 16H, CH_3, B-*H*). ^{13}C NMR (100 MHz, $CDCl_3$): δ (ppm) 139.4, 135.7, 130.7, 125.6, 122.3, 78.3, 62.8, 25.9 ppm. ^{11}B NMR (128 MHz, $CDCl_3$): δ (ppm) –1.0, –2.5, –3.8, –8.2, –9.4, –11.8, –12.7, –14.0. HRMS (APCI$^-$): Calcd. for $C_{10}H_{19}B_{10}Br$ $(M+Cl)^-$ m/z 363.1347, found m/z 363.1348.

General synthesis of *p*-(*o*-carboran-1-yl)diphenylaniline, 3a–c

The xylene solution of XPhos, **2**, diphenylamine, *t*-BuOK and $Pd(OAc)_2$ was stirred at 140 °C for 18 h under Ar atmosphere. After cooling to room temperature, the reaction was quenched by water. The products were extracted by $CHCl_3$, and then the organic layer was washed with water. After drying over $MgSO_4$, the solvent was evaporated. The residue was purified by column chromatography on a silica gel and HPLC, and the desired product was collected by freeze drying from a benzene solution.

3a.

White solid (9%).^{1}H NMR (400 MHz, $CDCl_3$): δ (ppm) 7.29 (s, 6H, Ar–*H*), 7.10 (1H, s, Ar–*H*), 6.90 (d, 2H, *J* = 9.0, Ar–*H*), 3.86 (s, 1H, carborane_C–*H*), 3.8–1.80 (br, 10H, B–*H*). ^{13}C NMR (100 MHz, $CDCl_3$): δ (ppm) 149.4, 146.8, 129.5, 128.7, 125.5, 125.5, 124.2, 120.9, 61.0, 29.7. ^{11}B NMR (128 MHz, $CDCl_3$): δ (ppm) –1.5, –2.6, –4.5, –5.4, –8.7, –9.9, –11.3, –12.2, –13.4. HRMS ($APCI^+$): Calcd. for $C_{20}H_{26}B_{10}N$ $(M+H)^+$ m/z 390.2996, found m/z 390.2990.

3b.

White solid (43%).^{1}H NMR (400 MHz, CD_2Cl_2): δ (ppm) 7.42 (d, 2H, *J* = 9.0 Hz, Ar–*H*), 7.31 (d, 4H, *J* = 7.9, Ar–*H*) 7.14–7.10 (m, 6H, Ar–*H*), 6.93 (d, 2H, *J* = 9.0, Ar-*H*), 3.2–1.8 (br, 10H, B–*H*), 1.73 (s, 1H, C*H*$_3$). ^{13}C NMR (100 MHz, $CDCl_3$): δ (ppm) 149.8, 146.6, 131.8, 129.6, 125.7, 124.4, 122.7, 120.3, 82.9, 77.6, 23.1, 23.1. ^{11}B NMR (128 MHz, CD_2Cl_2): δ (ppm) –4.3, –5.4, –9.0, –10.0, –11.1. HRMS ($APCI^-$): Calcd. for $C_{21}H_{26}B_{10}N$ $(M)^-$ m/z 402.2996, found m/z 402.3116.

3c.

White solid (4%).^{1}H NMR (400 MHz, CD_2Cl_2): δ (ppm) 7.45 (t, 4H, *J* = 7.70 Hz, Ar–*H*), 7.24 (t, 5H, *J* = 8.7, Ar–*H*) 6.83 (s, 2H, Ar–*H*), 5.48 (s, 1H, carborane_C–*H*),3.7–1.90 (br, 16H, C*H*$_3$ B–*H*). ^{13}C NMR (100 MHz, CD_2Cl_2): δ (ppm) 147.2, 147.1, 128.9, 134.1, 129.9, 125.8, 125.7, 124.4, 92.7, 80.2, 26.5, 26.4. ^{11}B NMR (128 MHz, CD_2Cl_2): δ (ppm) –2.1, –3.2, –4.3, –8.5, –9.7, –11.3, –12.8, –14.1. HRMS (APCI): Calcd. for $C_{22}H_{28}B_{10}N$ $(M-H)^-$ m/z 416.3152, found m/z 416.2969.

References

1. Yates, K.; Mandrapilias, G. *J. Org. Chem*. **1980**, *45*, 3902−3906.

2. Aoki, T.; Kobayashi, Y.; Kaneko, T.; Oikawa, E.; Yamamura, Y.; Fujita, Y.; Teraguchi, M.; Nomura, R.; Masuda, T. *Macromolecules* **1999**, *32*, 79−85.

Figures and Table

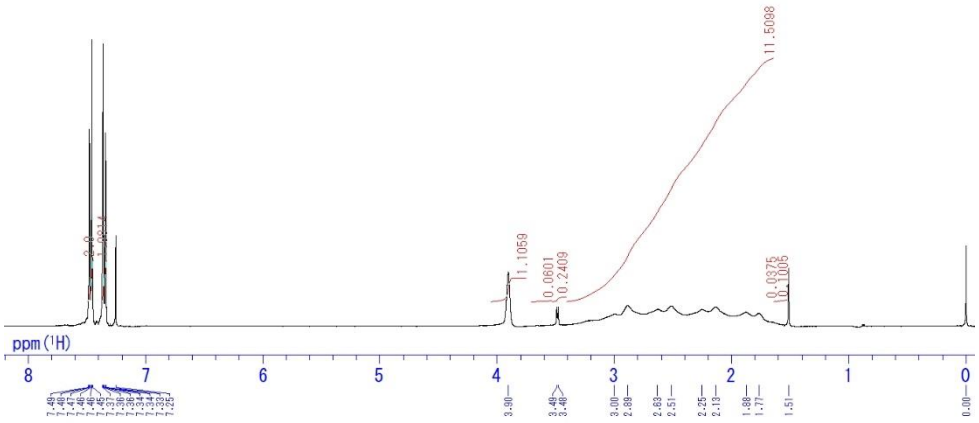

Chart S1. ^{1}H NMR spectrum of **2a** in $CDCl_3$ at room temperature.

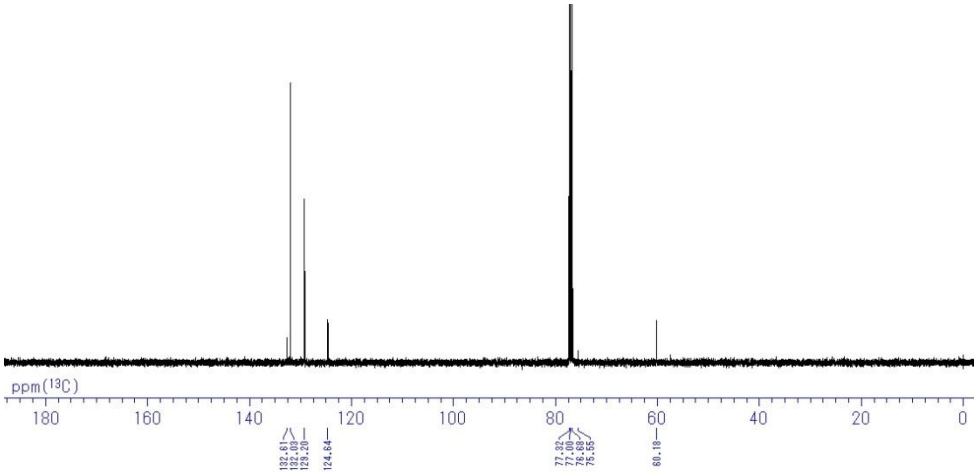

Chart S2. ^{13}C NMR spectrum of **2a** in $CDCl_3$ at room temperature.

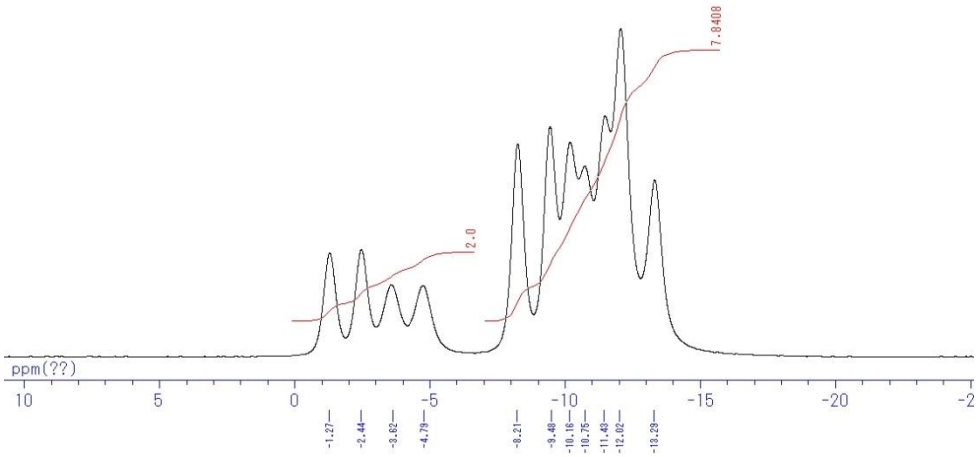

Chart S3. ^{11}B NMR spectrum of **2a** in $CDCl_3$ at room temperature.

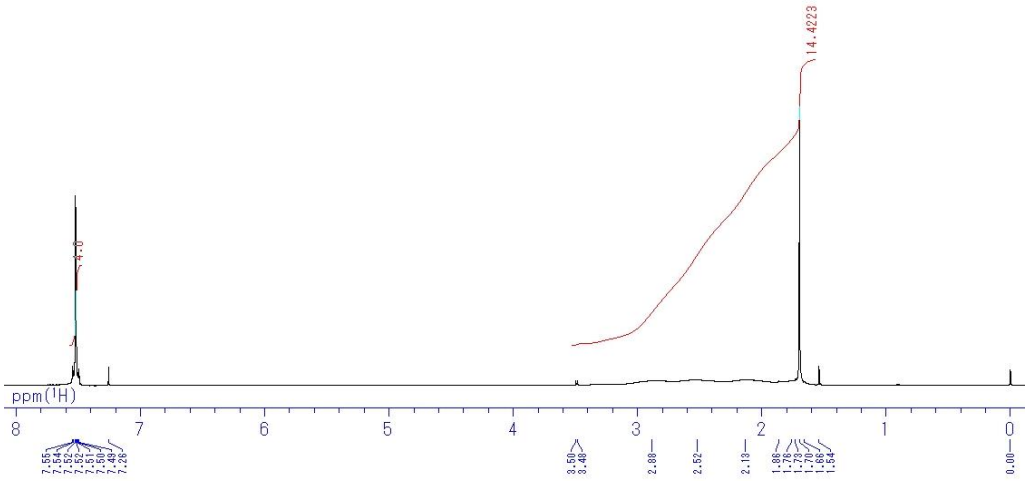

Chart S4. ^{1}H NMR spectrum of **2b** in $CDCl_3$ at room temperature.

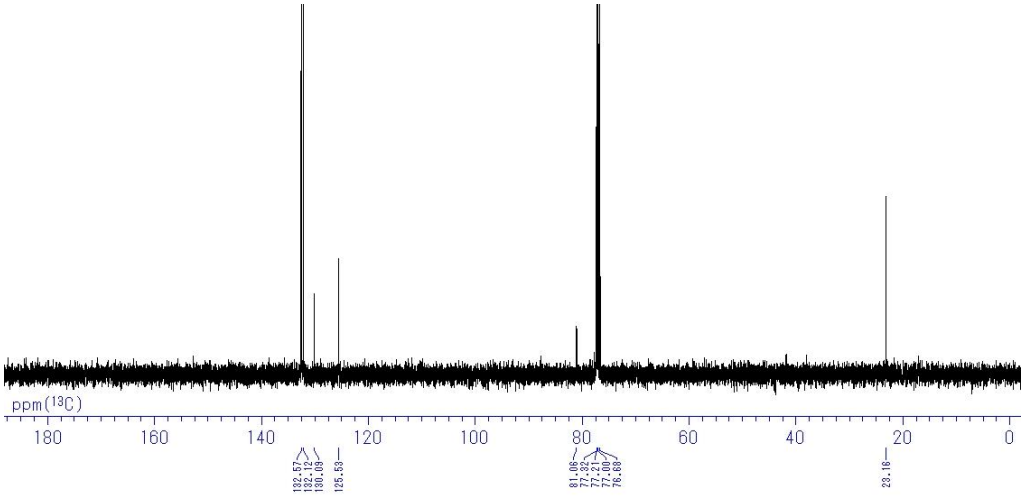

Chart S5. ^{13}C NMR spectrum of **2b** in $CDCl_3$ at room temperature.

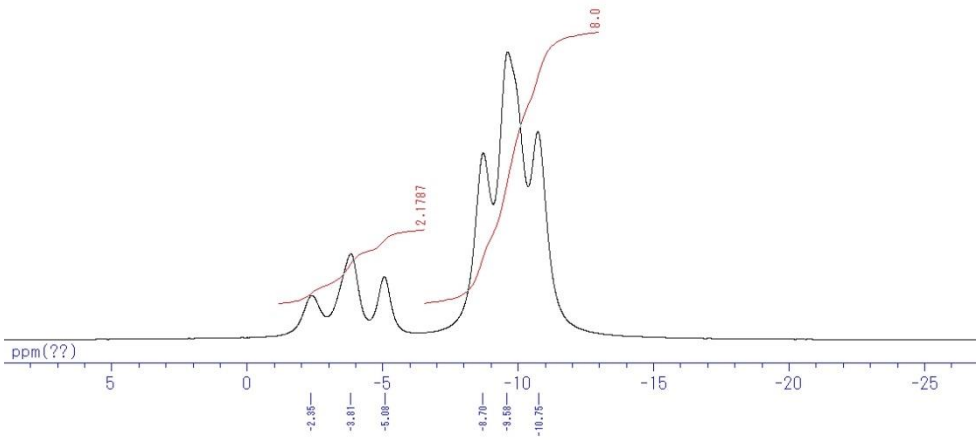

Chart S6. ^{11}B NMR spectrum of **2b** in $CDCl_3$ at room temperature.

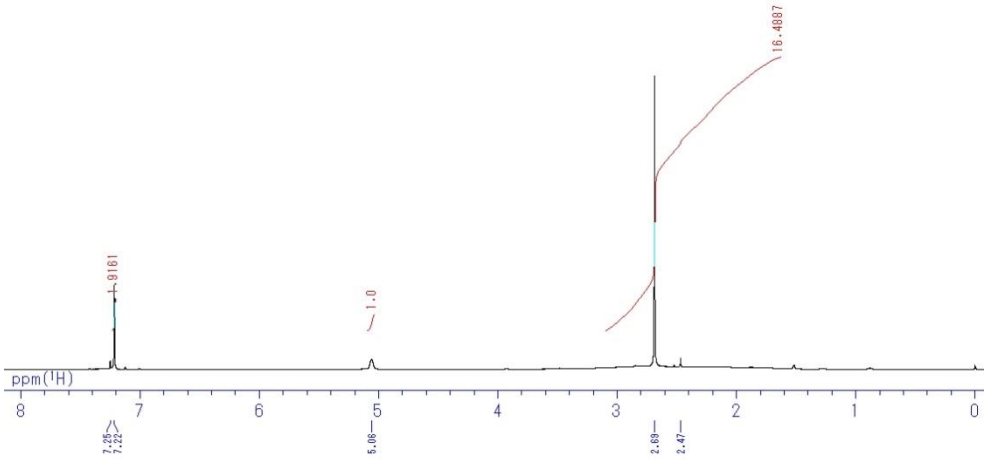

Chart S7. ^{1}H NMR spectrum of **2c** in $CDCl_3$ at room temperature.

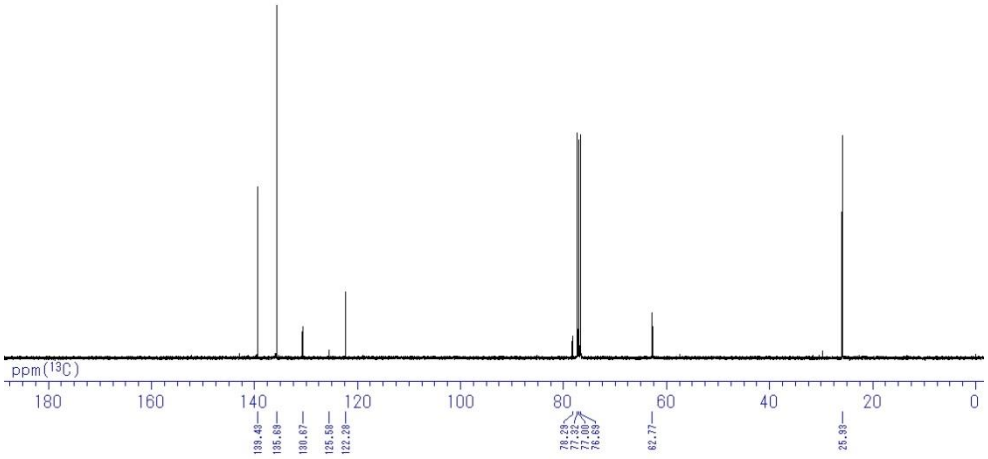

Chart S8. ^{13}C NMR spectrum of **2c** in $CDCl_3$ at room temperature.

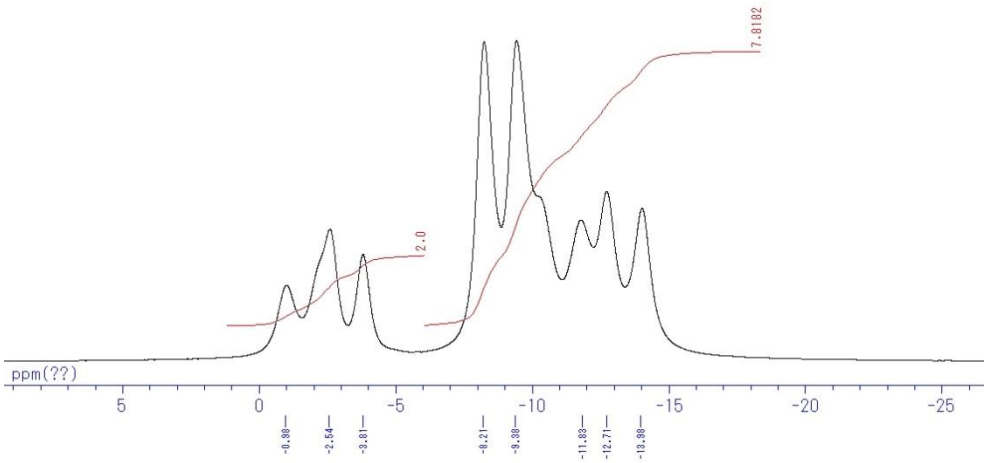

Chart S9. ^{11}B NMR spectrum of **2c** in $CDCl_3$ at room temperature.

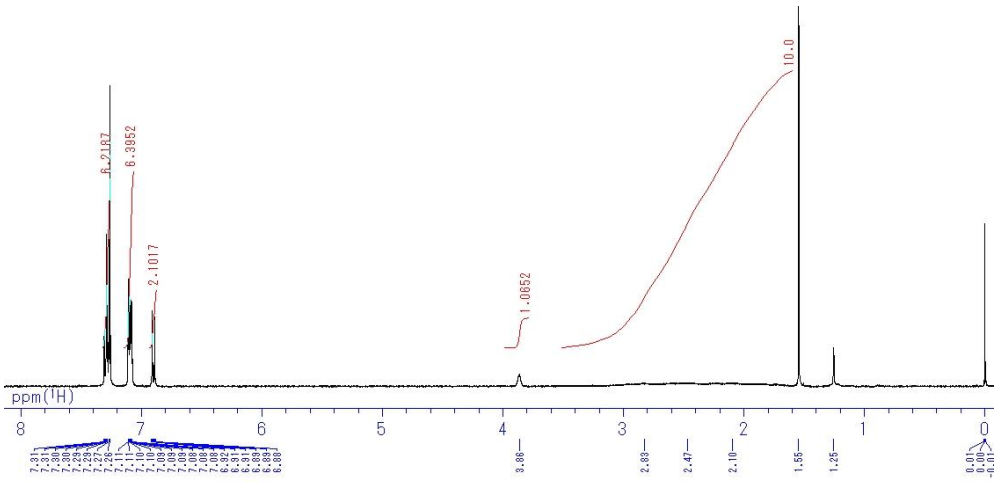

Chart S10. ^{1}H NMR spectrum of **3a** in $CDCl_3$ at room temperature.

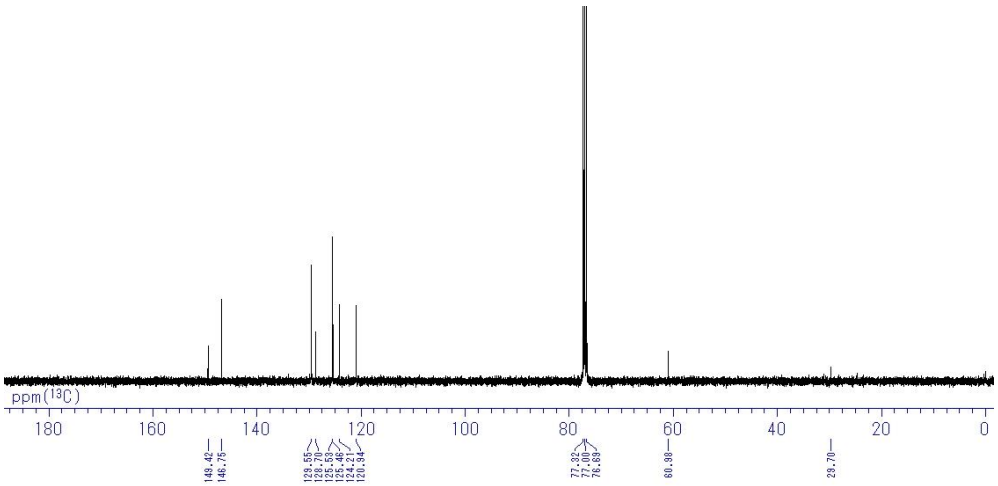

Chart S11. ^{13}C NMR spectrum of **3a** in $CDCl_3$ at room temperature.

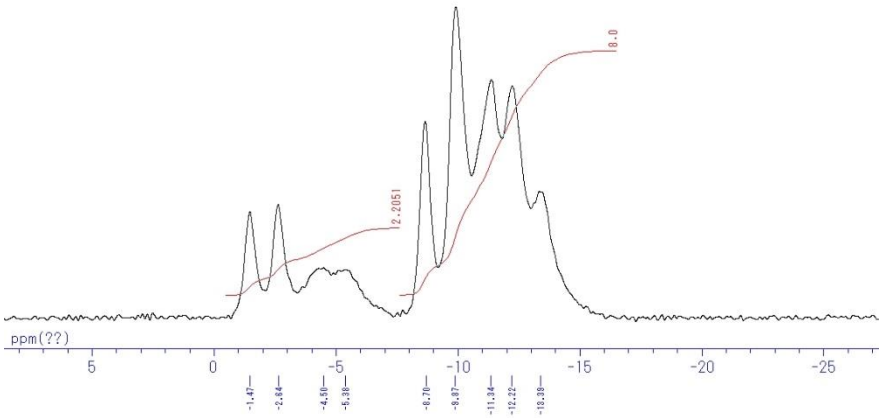

Chart S12. ^{11}B NMR spectrum of **3a** in $CDCl_3$ at room temperature.

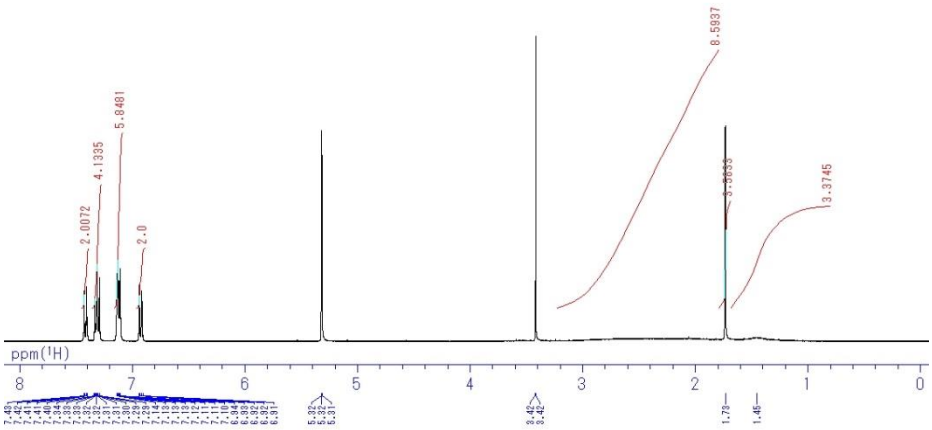

Chart S13. ^{1}H NMR spectrum of **3b** in CD_2Cl_2 at room temperature.

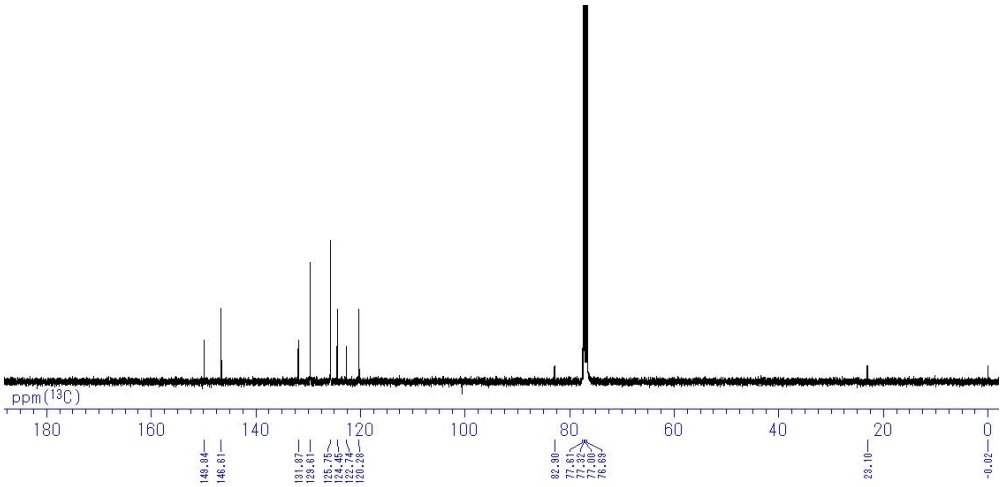

Chart S14. ^{13}C NMR spectrum of **3b** in CD_2Cl_2 at room temperature.

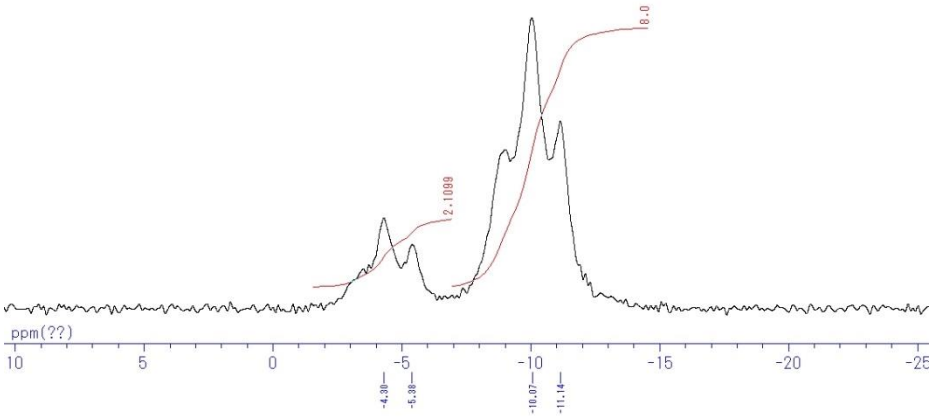

Chart S15. ^{11}B NMR spectrum of **3b** in CD_2Cl_2 at room temperature.

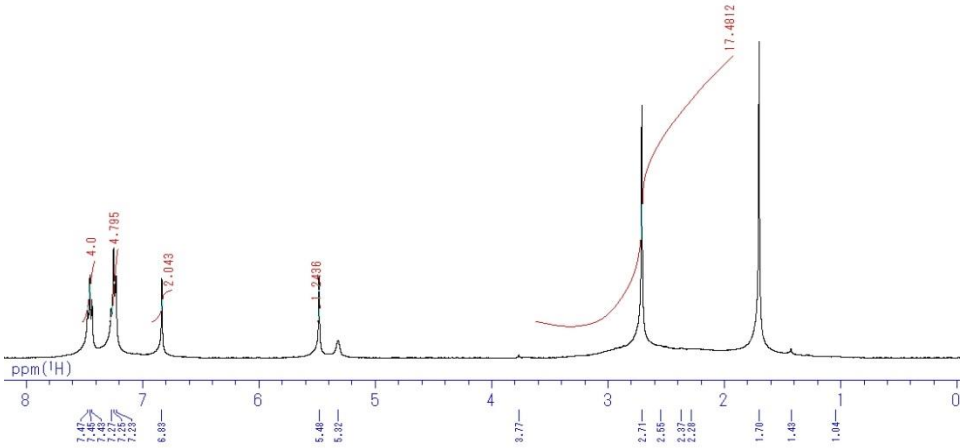

Chart S16. ^{1}H NMR spectrum of **3c** in CD_2Cl_2 at room temperature.

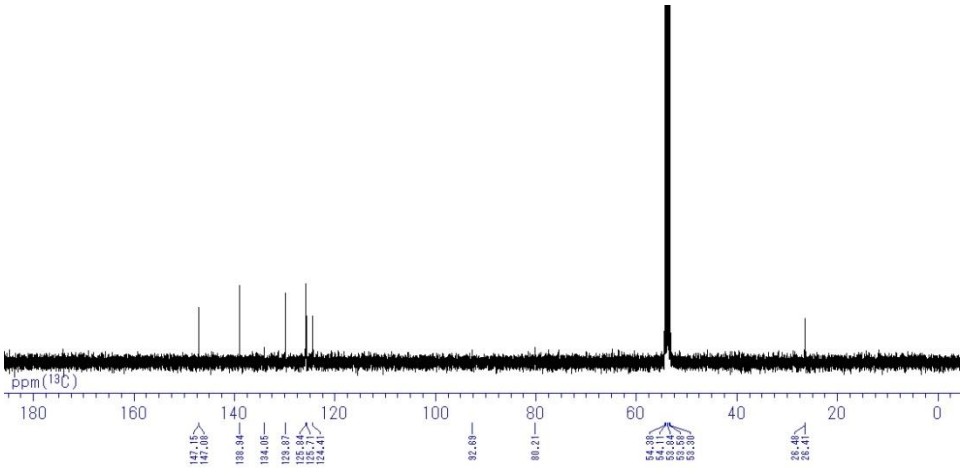

Chart S17. ^{13}C NMR spectrum of **3c** in CD_2Cl_2 at room temperature.

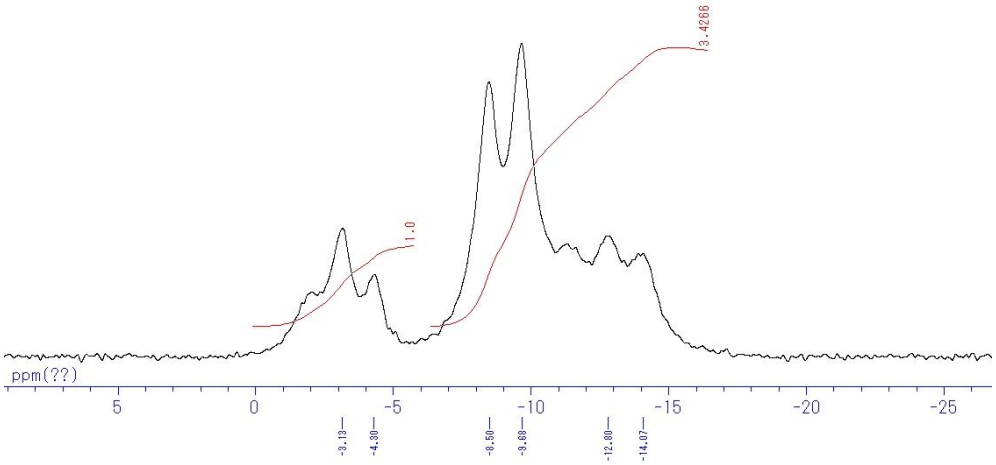

Chart S18. ^{11}B NMR spectrum of **3c** in CD_2Cl_2 at room temperature.

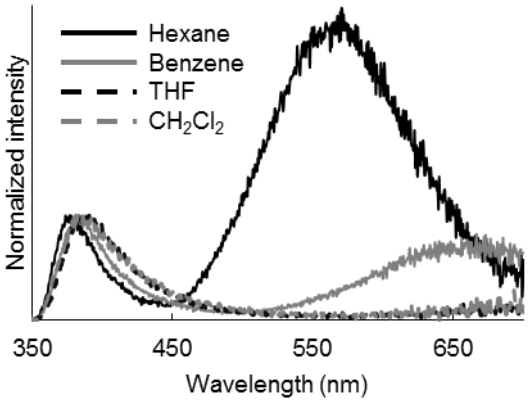

Figure S1. Solvent dependent photoluminescence spectra of **3a** (1.0×10^{-5} M).

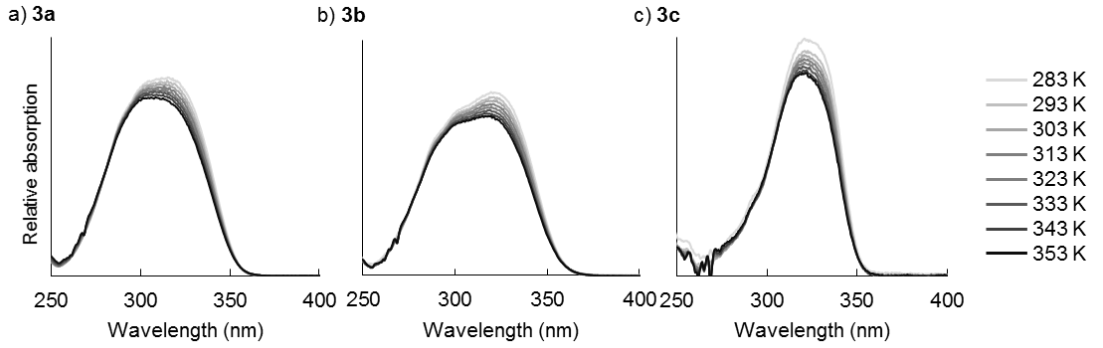

Figure S2. Variable-temperature UV–vis absorption spectra of **3a–c** in octane (1.0×10^{-5} M).

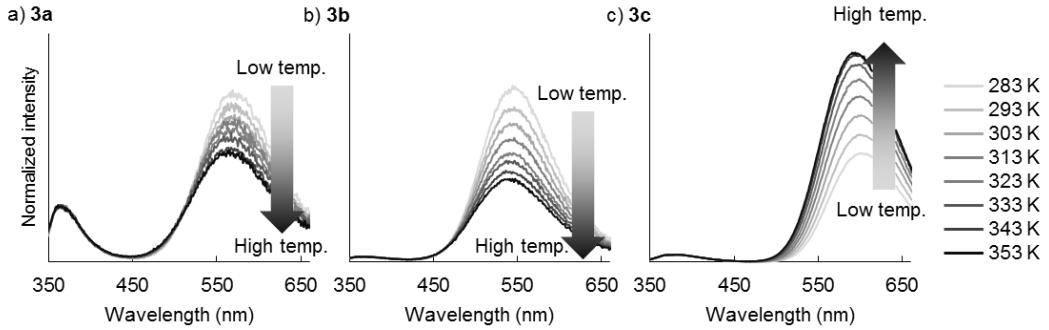

Figure S3. Variable temperature photoluminescence spectra of **3a** (left), **3b** (center) and **3c** (right) in octane (1.0×10^{-5} M).

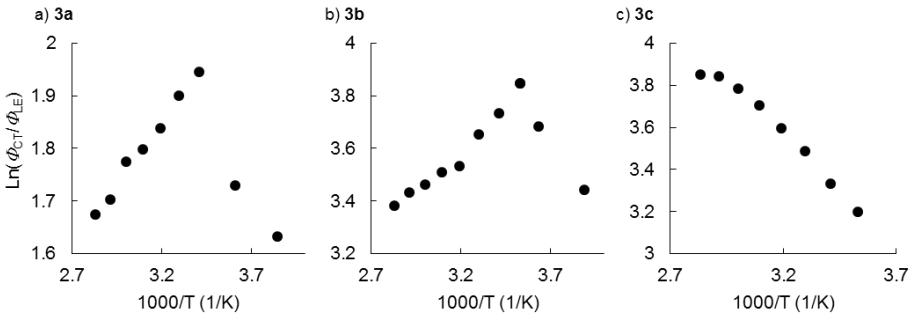

Figure S4. Stevens–Ban plots with **3a–c**.

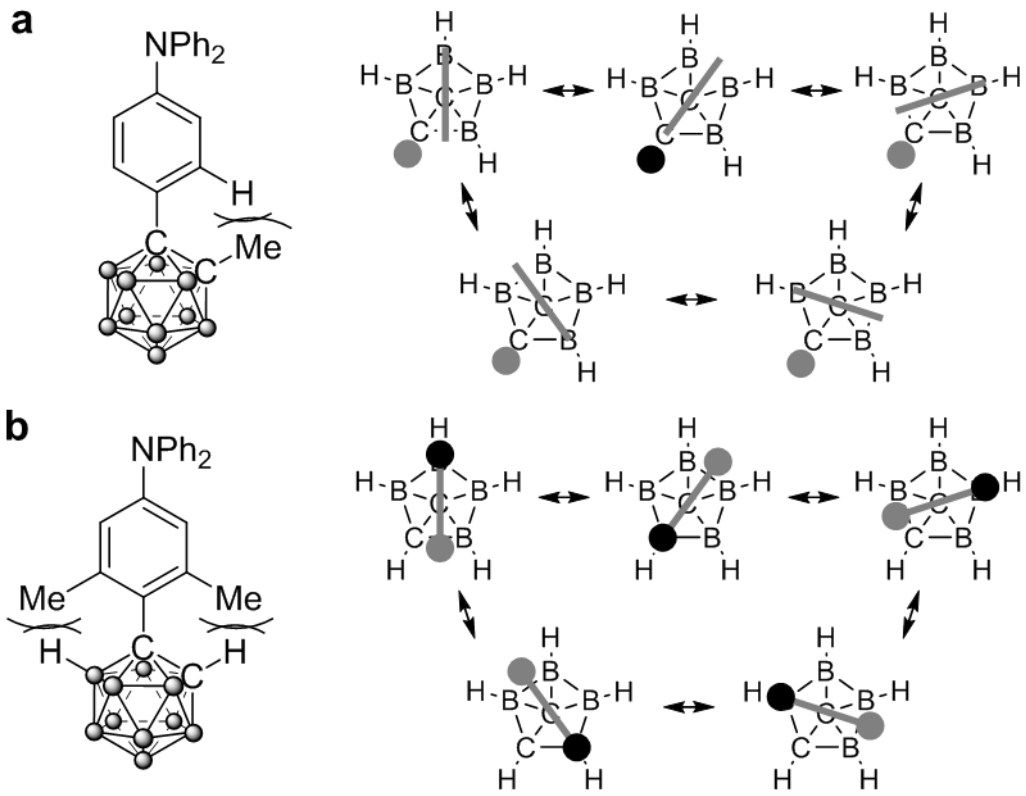

Figure S5. Schematic intramolecular steric hindrances of (a) **3b** and (b) **3c** between methyl groups and *o*-carborane. C_5 symmetric *o*-carborane and the benzene ring of triphenylamine (grey bar). Black and gray balls represent the methyl group with or without steric hindrances, respectively.

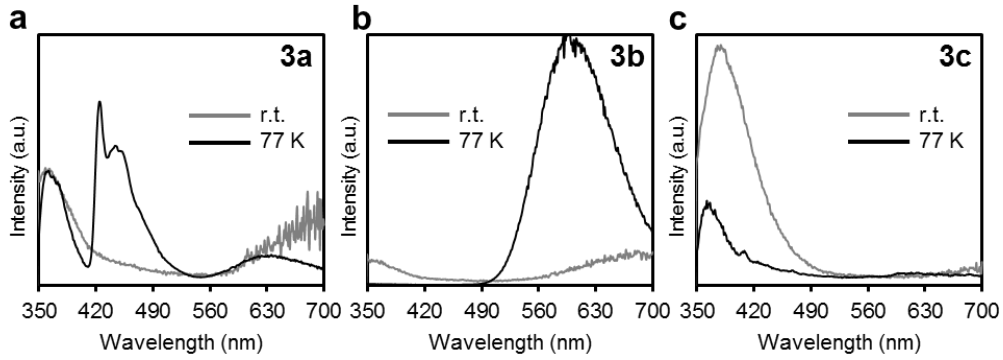

Figure S6. PL spectra of **3a**–**c** in 2-methylTHF at r.t. (gray line) and 77 K (black line) with the concentration at 1.0×10^{-5} M.

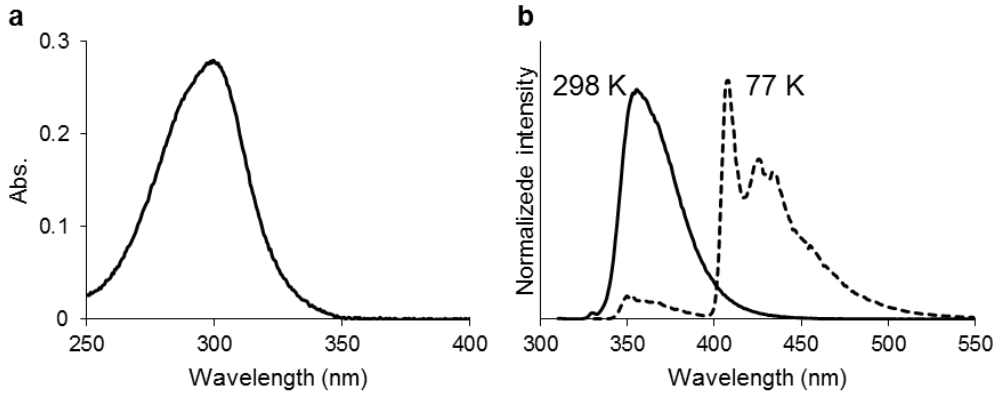

Figure S7. (a) UV−vis absorption and (b) photoluminescence spectra of triphenylamine in octane and 2-MeTHF, respectively (1.0×10^{-5} M).

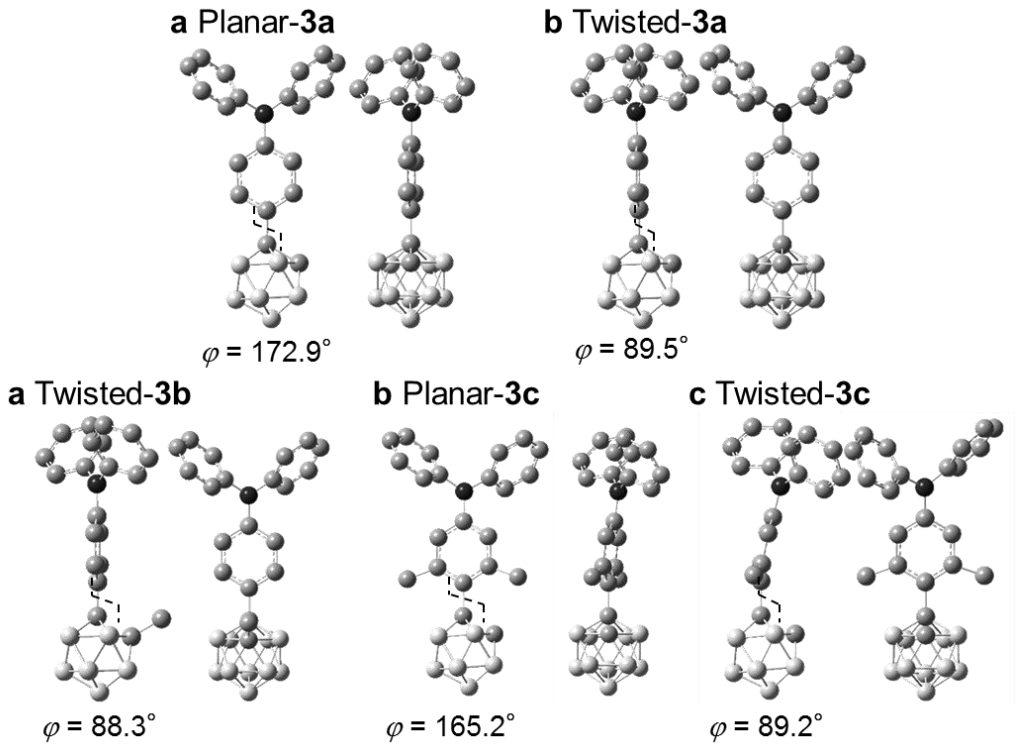

Figure S8. Optimized structures of planar and twisted conformations of **3** in the ground state. Hydrogen atoms were omitted for clarity.

Table S1. Predicted absorption transitions of **3a**

	Planar			Twisted		
excited state	transition	λ_{calc} (nm)	f	transition	λ_{calc} (nm)	f
$S_0 \rightarrow S_1$	H → L (76%) H → L+1 (12%)	297.00	0.4061	H → L (91%)	295.89	0.5701
$S_0 \rightarrow S_2$	H → L (13%) H → L+1 (76%)	295.43	0.1566	H → L+1 (88%)	292.19	0.0326
$S_0 \rightarrow S_3$	H → L+2 (68%) H → L+3 (24%)	277.12	0.2136	H → L+2 (75%) H → L+3 (18%)	275.33	0.1945
$S_0 \rightarrow S_4$	H → L+4 (34%) H → L+5 (36%)	256.61	0.0338	H → L+4 (25%) H → L+5 (44%)	254.43	0.0321

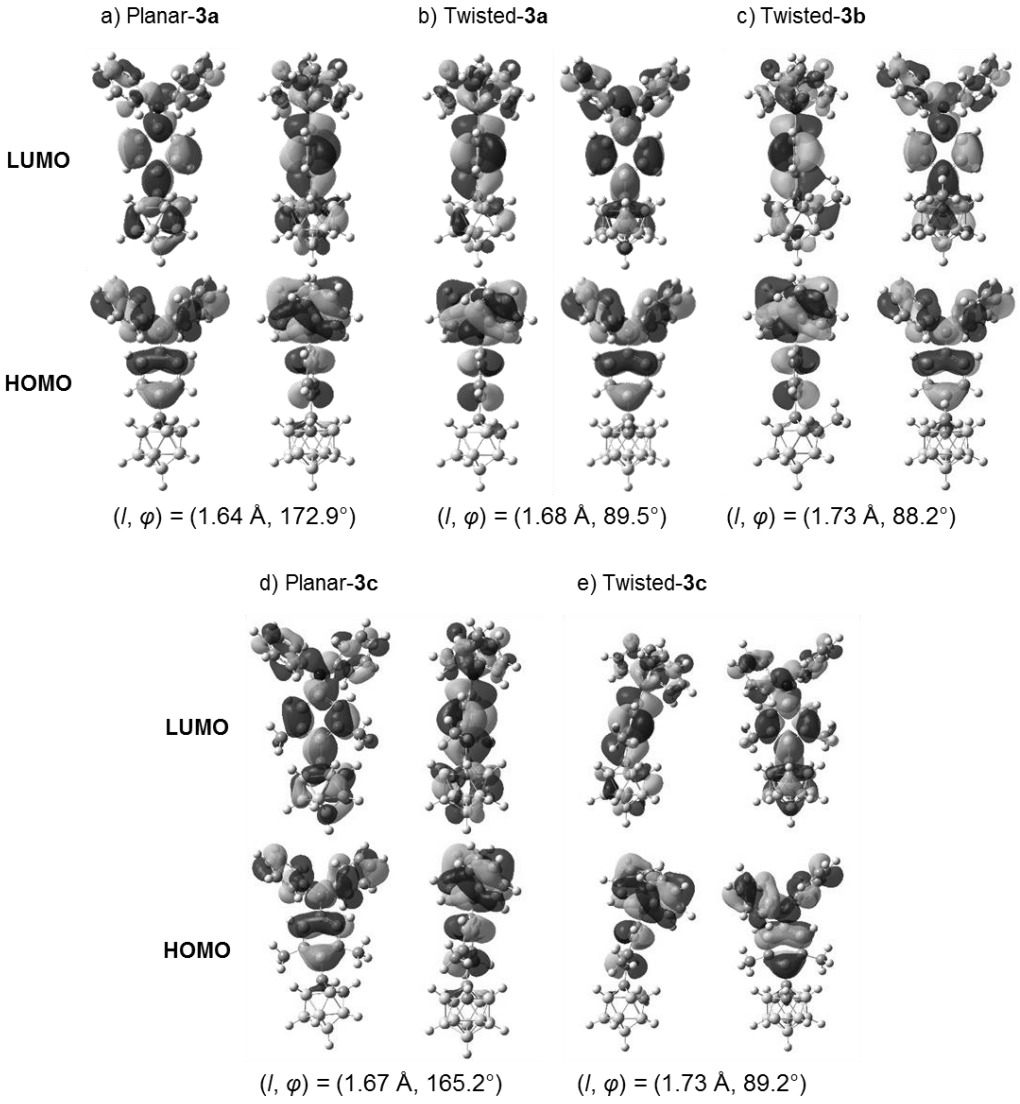

Figure S9. HOMOs and LUMOs of *o*-carborane derivatives.

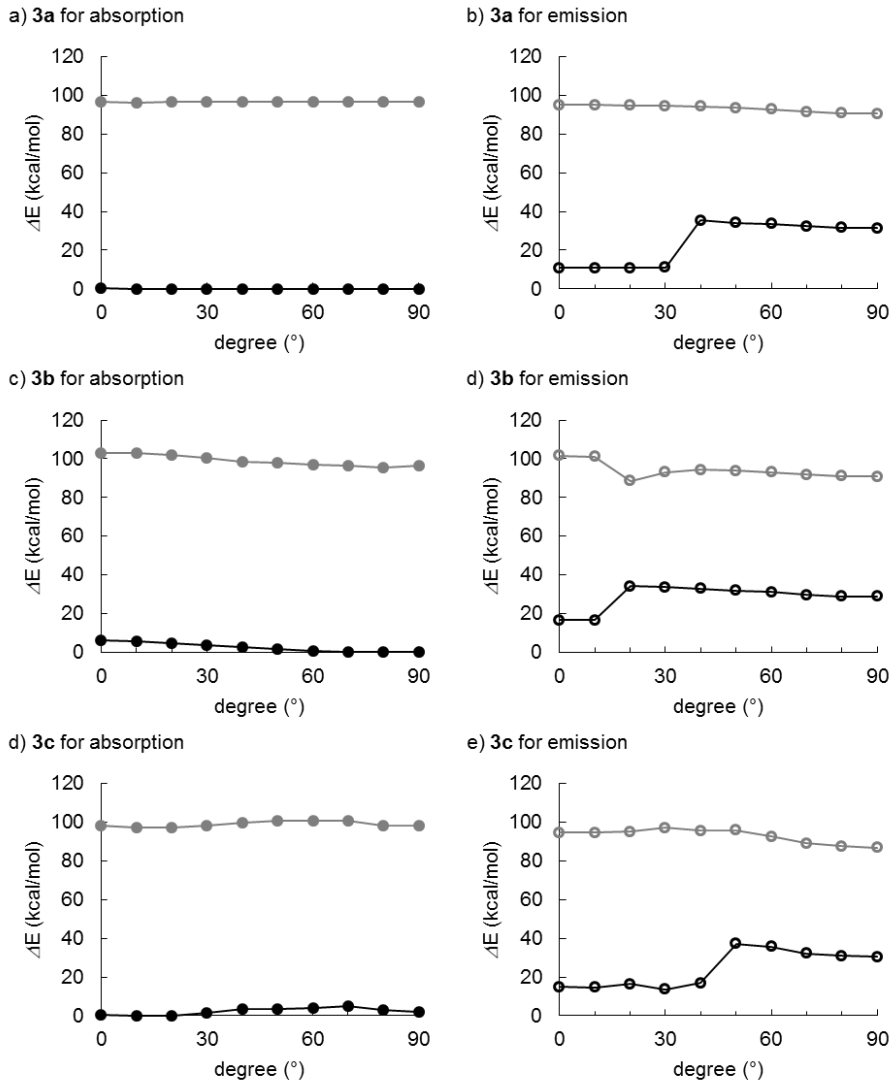

Figure S10. Energy diagrams of **3a-c** with different dihedral angles (φ) in a, c, e) absorption S_0–S_1 and b, d, f) emission S_1'–S_0' transitions. Black and gray dots mean the calculated S_0 and S_1 states, respectively. Black and gray circles mean the calculated S_0' and S_1' states, respectively.